

3D HYBRID-PIC SIMULATION OF PLASMA EXPANSION IN THE PRESENCE OF A DIPOLE MAGNETIC FIELD

H. B. Nersisyan,^{*1,2} K. A. Sargsyan,¹ D. A. Osipyan,¹ M. V. Sargsyan,¹ H. H. Matevosyan¹

¹*Department of Theoretical Physics, Institute of Radiophysics and Electronics, 0203 Ashtarak, Armenia*

²*Centre of Strong Fields Physics, Yerevan State University, Alex Manoogian str. 1, 0025 Yerevan, Armenia*

E-mail: hrachya@irphe.am

Received 30 July, 2011

Abstract—The collisionless interaction of an expanding high-energy plasma cloud with a magnetized background plasma in the presence of a dipole magnetic field is examined in the framework of a 3D hybrid (kinetic ions and massless fluid electrons) model. The retardation of the plasma cloud and the dynamics of the perturbed electromagnetic fields and the background plasma are studied for high Alfvén-Mach numbers using the particle-in-cell method. It is shown that the plasma cloud expands excluding the ambient magnetic field and the background plasma to form a diamagnetic cavity which is accompanied by the generation of a collisionless shock wave. The energy exchange between the plasma cloud and the background plasma is also studied and qualitative agreement with the analytical model suggested previously is obtained.

Keywords: magnetized plasma, dipole magnetic field, vortices, shock waves, numerical simulations

1. Introduction

When high-energy density plasma is expanded into magnetized background plasma, the injected plasma expands and excludes the background plasma and magnetic field to form a diamagnetic cavity. This process has been observed in a number of experiments in space and the laboratory (e.g., [1] and references therein). The similar processes are responsible for the formation of the heliopause, where solar wind drags or convects magnetic fields from the Sun, which causes the deflection of both the interstellar medium and cosmic rays. Other examples of naturally occurring inflated or stretched magnetic fields include coronal mass ejections and the formation of the Earth's magnetotail [2-4]. Starting in the 1960s, many experiments of the collisionless phenomena of exploding plasmas in space and laboratory were performed or planned. Dense, high-energy plasmas can also be formed by laser irradiation of a small target embedded in a gas in an external magnetic field [5]. The background gas can either be pre-ionized or be ionized by the laser. Such experiments show that, in addition to expansion, the target plasma is also subject to flute instabilities on its surface as it interacts with the background field and embedded plasma. The diamagnetic cavities are expected to occur also in supernova explosions [6]. The physics of the plasma expansion and evolution has been investigated in detail numerically, using a variety of techniques, such as full particle [7], hybrid (particle ions, fluid electron) [8-10] and magnetohydrodynamics (MHD) [11] codes. The properties of the expansion phase in the presence of either a stationary [12] or flowing background plasma [13], as well as the details of unstable modes on the surface of the expanding plasma [13-15], have been well studied.

Typical experimental parameters are such that the ions are collisionless but the situation for the electrons ranges from collisionless to collision-dominated. In this paper the dynamics of the expanding plasma cloud is studied for the completely collisionless regimes, which, in particular, are realized in many astrophysical processes (e.g., [1] and references therein). An example is the problem of the collisionless retardation of the supernovae remnants which was first formulated by [16] and subsequently analyzed in detail by [17].

In recent years, the basic concept of the plasma expansion has been extended to consider a large magnetic bubble, which can be formed using a small magnetic coil and plasma source attached to a spacecraft, to efficiently inflate the bubble to a large cross-sectional area [3, 18]. A net force would be exerted on the spacecraft due to the deflection of the solar wind around the bubble. In this case, the plasma is continuously injected in the presence of a dipole or dipole-like magnetic field. Theoretical arguments [19] and calculations (e.g., [3, 20, 21] and references therein) suggest that the magnetic field of the dipole can be expanded with the plasma, so that the magnitude of the field falls off much slower with distance r from the dipole, namely as r^{-s} , with $s \sim 1, 2$ in certain directions at least, rather than r^{-3} (for a bare dipole), allowing a large bubble to form. Laboratory experiments [22, 23] have provided some evidence for the slow falloff of the field from the source. However, the nature of the plasma and magnetic field expansion in this configuration is not completely understood, and how it compares with the more common picture of diamagnetic cavity formation has not been addressed to date. Some papers [1,2,9,10,20] and the references cited therein conducted a systematic study in a two-dimensional (2D) geometry and only for initial phase of expansion [2], and in a three dimensions (3D) but mainly of the characteristics of the magnetic field inflation [20]. Special attention has been paid to the MHD analysis of the expanding plasma behavior in a dipole field in a vacuum [24], i.e. in the absence of the background plasma.

In this paper, in order to provide further insight into the underlying physics we have performed systematic particle-in-cell (PIC) 3D hybrid simulations of the plasma expansion in a magnetized background plasma in the presence of a dipole magnetic field. The basic parameters of the problem are introduced in Sec. 2. The numerical method and model used are discussed in Sec. 3. We perform a number of simulations assuming hydrogen cloud and hydrogen background plasmas and the results are presented and discussed in Sec. 4. Finally, we state the conclusions in Sec. 5.

2. Basic Parameters for the Plasma Expansion

The plasma expansion process is characterized by the magnetic (R_m) and hydrodynamic (R_g) retardation lengths. R_m is obtained by equating the initial kinetic energy W_0 of an initially spherical plasma cloud to the energy of the magnetic field that it pushes out in expanding to the radius R_m [25], i.e., $R_m = (6W_0/H_0^2)^{1/3}$. Here H_0 is the strength of the unperturbed magnetic field. As the

plasma expands, it draws the background plasma into a combined motion. Along with this, the mass of expelled plasma increases. The radius of the sphere within which the mass of the plasma cloud and that of the background plasma drawn into the combined motion become equal is referred to as the hydrodynamic retardation length: $R_g = (3M/4\pi n_b m_b)^{1/3}$, where n_b and m_b are the density and mass of the background plasma ions [17] and M is the mass of the expanding plasma. The smaller of the lengths, R_m or R_g , determines the predominant mechanism for the retardation of the plasma cloud – magnetic or hydrodynamic. Of course R_m and R_g account for the ideal characteristics of the retardation process, therefore some high-energy particles may penetrate beyond the stopping length. The relation $R_m/R_g \sim M_A^{2/3}$, where $M_A = u/v_A$ is the Alfvén–Mach number ($u \sim (W_0/M)^{1/2}$ is the initial expansion velocity of the plasma) and $v_A = H_0/\sqrt{4\pi n_b m_b}$ is the Alfvén velocity in the background plasma, implies that for $M_A \ll 1$ the cloud loses energy as a result of the deformation and displacement of the magnetic field, while for $M_A \gg 1$ the retardation is caused by the interaction with the background plasma [9, 10, 26] (see also [1]). In this paper we consider only the second (hydrodynamic) regime of collisionless expansion with $M_A > 1$. In this case the retardation length is given by $l_s \approx R_g$.

An analysis shows that the hydrodynamic retardation can only be ensured by a collisionless laminar (or turbulent) mechanism [26] associated with the generation of vortical electric fields E_i in the front of the expanding plasma or by a collisional mechanism owing to pairwise collisions of the cloud ions with the ions and electrons of the background plasma. The ions of the expanding plasma transfer their energy to the ions and electrons of the background plasma in multiple ion-ion or ion-electron Coulomb collisions with a mean free paths λ_{ii} and $\lambda_{ei} \sim (m_e/m_c)\lambda_{ii}$, respectively [27, 28]. Here m_e and m_c are the electron and cloud ion masses, respectively. In this paper we assume a completely collisionless regimes when $\lambda_{ii} \gg \lambda_{ei} > l_s$. Strictly speaking, the hydrodynamic description is inapplicable under these conditions. However, as shown in [29], the hydrodynamic approach, when considering collisionless plasma expansion into the magnetized, ionized medium, can give quite reasonable qualitative and even satisfactory quantitative results. The physical reason underlying this situation is the small ion cyclotron radius a_L in comparison with a characteristic flow scale l_s , with the ion cyclotron radius playing the role of particle mean free path.

The first group of the collisionless interaction mechanisms are collective turbulent mechanisms (anomalous viscosity, anomalous resistivity) during the development of ion–ion or electron–ion beam instabilities [30]. The condition for excitation of the ion–ion instability has the form $u^2 \leq v_A^2 + 2c_s^2$ (see, e.g., [31]) or $M_A^2 \leq 1 + 2c_s^2/v_A^2$, where $c_s = \sqrt{T_e/m_b}$ is the ion sound speed

in the background plasma. In many typical situations $v_A \gtrsim c_s$ and $M_A \lesssim 2$. Thus, according to the criteria mentioned above at high Alfvén-Mach numbers $M_A \gg 1$ the retardation of the expanding plasma cannot be caused by the turbulent mechanisms.

The second group is the collisionless laminar retardation mechanism associated with the generation of vortical electric fields. It is known that the role of vortical electric fields becomes predominant as M_A increases, since $E_i/E_p \sim M_A^2$ [26], where E_p is the polarization electric field which arises as a result of the drop of the hydrodynamic and magnetic pressures at the front of the plasma cloud. A model for energy exchange between the cloud and the background plasma due to the combined effect of the gyromotion of the ions and the generation of vortical electric fields when $M_A > 1$ (so-called magnetolaminar mechanism (MLM)) has been proposed in [32]. Analytic solutions for the initial expansion phase, when only a vortical electric field E_i develops, showed that the fraction of energy transferred from the cloud to the background plasma is proportional to $\delta = (R_g/a_L)^2$ (MLM interaction parameter), where a_L is the cyclotron radius of the cloud ions.

In the framework of the ideal MHD approximation for the description of the plasma expansion into a vacuum in the presence of dipole magnetic field, another energetic parameter κ was defined which is given by $\kappa = W_0/W_m$ [33], where W_m is the total magnetic energy of the dipole beyond the spherical radius r_d ($W_m = p^2/3r_d^3$), r_d is the distance from the dipole to the center of the plasma cloud and p is the magnetic moment magnitude. Nikitin et al. introduced critical value κ_c for a different plasma location [33]. In the case when $\kappa < \kappa_c$ a substantial plasma retardation will occur in all directions from the cloud center location ("quasi-capture" mode), meanwhile the plasma will not be captured by an ambient magnetic field when $\kappa > \kappa_c$ ("rupture" mode). The critical value varies between 0.1 and 0.4. The latter value is realized when the plasma cloud is located at the dipole axis. In this paper we consider only the second regime of the plasma expansion.

3. Collisionless hybrid simulation

The hybrid model is used to study the collisionless plasma expansion in a magnetic field. This model describes the ions by means of the velocity distribution function $f(\mathbf{r}, \mathbf{v}, t)$, the electrons being considered hydrodynamically [34,35]. The typical scale on which the macroscopic parameters (the plasma density, magnetic field) vary is the ion cyclotron radius a_L . The electron cyclotron radius a_{Le} is much less than a_L due to the small electron mass. Of course, the electron distribution function changes sharply on a small scale a_{Le} , but we do not consider such details. If we are interested in the behavior of those macroscopic parameters that vary on a scale a_L , it is sufficient to

consider only the motion of the electron small-scale gyromotion centers. In this case one can consider the electrons as a fluid and describe their motions hydrodynamically.

All of the estimates show that the plasma under the conditions in question is essentially quasineutral everywhere, although there are thin space charge regions. These regions are located near the plasma cloud boundary as well as near the collisionless shock in the background plasma. The scales of these regions are essentially less than a_L , and therefore, they are not considered here. Then the densities of ions n_α and electrons n_e in quasineutral plasma satisfy the condition $n_e = \sum_\alpha Z_\alpha n_\alpha$, where $Z_\alpha e$ is the charge of the ion from plasma species α . Let the cloud ions have the index $\alpha = c$, whereas the index of the background ions is $\alpha = b$. The ion distribution functions f_α are governed by the Vlasov kinetic equation

$$\frac{\partial f_\alpha}{\partial t} + \mathbf{v} \cdot \frac{\partial f_\alpha}{\partial \mathbf{r}} + \frac{Z_\alpha e}{m_\alpha} \left(E + \frac{1}{c} [\mathbf{v} \times \mathbf{H}] \right) \frac{\partial f_\alpha}{\partial \mathbf{v}} = 0. \quad (1)$$

The electric and magnetic fields satisfy the Maxwell equations

$$\nabla \times \mathbf{H} = \frac{4\pi n_e e}{c} (\mathbf{v}_i - \mathbf{v}_e), \quad \nabla \times E = -\frac{1}{c} \frac{\partial \mathbf{H}}{\partial t}, \quad (2)$$

in which the displacement current is omitted. We assume non-relativistic expansion velocity of the plasma cloud. Here \mathbf{v}_i is the ion mean velocity which is defined as

$$n_e = \sum_\alpha Z_\alpha n_\alpha, \quad \mathbf{v}_i = \frac{1}{n_e} \sum_\alpha Z_\alpha n_\alpha \mathbf{v}_\alpha, \quad (3)$$

$$n_\alpha = \int f_\alpha d\mathbf{v}, \quad \mathbf{v}_\alpha = \int \mathbf{v} f_\alpha d\mathbf{v}. \quad (4)$$

The mean electron velocity \mathbf{v}_e satisfies the equation

$$\mathbf{E} = -\frac{1}{c} [\mathbf{v}_e \times \mathbf{H}], \quad (5)$$

which can be derived from the hydrodynamic equation of motion of electrons ignoring the inertial term (i.e. formally by taking the limit $m_e \rightarrow 0$). The electric field in Eq. (5) is that required to keep the electrons and ions together ensuring the quasineutrality of the plasma. Thus, we do not resolve the expansion process on the Debye scale. One can interpret Eq. (5) as follows. The electromagnetic force acting on the electrons and ions does not depend on the particle mass; therefore light electrons are accelerated much more than ions. This would lead to charge separation and would violate the quasineutrality condition if the strong Coulomb interaction would not prevent this from occurring; i.e., an appropriate electric field arises to enforce quasineutrality. The mean force itself, which so strongly accelerates the electron gas, has to disappear or, more exactly, its electric component has to compensate the Lorentz force within the accuracy of the order of m_e/m_α . This fact is expressed by

the approximate relation (5). Equations (1)–(5) constitute a closed system and are used to investigate the collisionless plasma dynamics in an external magnetic field.

Note that in Eqs. (1)–(5) we have also neglected the terms associated with the finite conductivity (e.g. magnetic field diffusion and Joule heating). It can be shown that this approximation is easily satisfied in a wide range of parameters. In fact, for example, we can estimate the characteristic diffusion time for the magnetic field, $\tau_m = 4\pi a_L^2 \sigma / c^2$, where a is the conductivity of the plasma. Introducing the characteristic retardation time of the plasma cloud $\tau_s = R_g / u$ we obtain $\tau_m / \tau_s \sim M_A^2 (\lambda_{ii} / R_g)$. Here λ_{ii} is the mean free path for ion–ion Coulomb interaction.

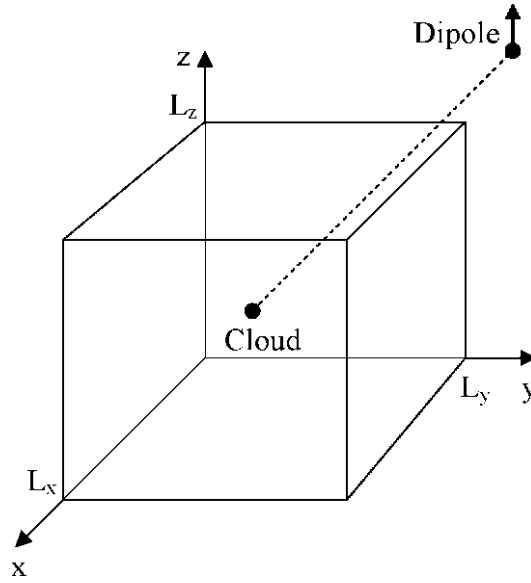


Fig. 1. Scheme of the simulation region showing location of the dipole and the initial position of the plasma cloud.

These approximations constitute the hybrid collisionless plasma model employed in this paper. It should be emphasized that earlier simulations and experiments demonstrated the practical realizability of the magnetolaminar interaction model [1, 26] discussed briefly in Sec. 2. In addition it can be shown that Eqs. (1)–(5) of the hybrid model have universal nature. This universality can be demonstrated by normalizing Eqs. (1)–(5) and all the quantities with the scales n_{b0} (densities), c/ω_{pb} (lengths), v_A (velocities), H_0 (magnetic field), $(v_a/c)H_0$ (electric field). In these units the time and the ionic distribution functions are scaled by the cyclotron period Ω_b^{-1} and n_{b0}/v_a^3 , respectively. Here ω_{pb} , Ω_b and n_{b0} are the plasma and cyclotron frequencies and the unperturbed (initial) density of the background ions, respectively. v_A is the Alfvén velocity in the background plasma. Then it is seen that Eqs. (1)–(5) depend only on the dimensionless parameters Z_c/Z_b and $Z_c m_b / Z_b m_c$.

Consider the dynamics of a point explosion that forms a cloud of dense plasma expanding into a magnetized low-density background plasma. For a simplicity we assume hydrogen cloud and background plasmas with $m_c = m_b = m_p$, $Z_c = Z_b = 1$, where m_p is the proton mass. At the initial time $t = 0$, an explosion occurs at the point $x_0 = L_x/2$, $y_0 = L_y/2$, $z_0 = L_z/2$ in a cubic region $0 \leq x \leq L_x$, $0 \leq y \leq L_y$, $0 \leq z \leq L_z$, (see Fig. 1) filled with a homogeneous background plasma of density n_{b0} . The magnetic dipole with a moment $\mathbf{p} = p_z \mathbf{e}_z$ creates a magnetic field $\mathbf{H}_0(\mathbf{r})$ and is placed outside the cubic region on the axis parallel to the x -axis ($x_d < 0$, $y_d = y_0$, $z_d = z_0$). We have also introduced the spherical coordinates r , θ , φ with the radius vector \mathbf{r} . The center of this coordinate system coincides with the initial position of the cloud and θ is the angle between \mathbf{r} and the cloud-dipole axis. φ is measured from the plane containing the plasma cloud and the dipole moment \mathbf{p} . We consider the case when the dipole moment is parallel to the z -axis and due to the symmetry we chose $p_z > 0$. In our simulations the dipole magnetic field is determined by the ratio $\eta = H_{0z}(0, y_0, z_0)/H_{0z}(L_x, y_0, z_0) > 1$ and the strength of the dipole magnetic field at the center of the simulation domain, i.e. $H_0 = -H_{0z}(x_0, y_0, z_0) > 0$. Using these two quantities it is easy to obtain the position x_d and the moment p_z of the dipole

$$p_z = \frac{L_x^3}{8} \left(\frac{\eta^{1/3} + 1}{\eta^{1/3} - 1} \right)^3 H_0, \quad x_d = -\frac{L_x^3}{\eta^{1/3} - 1}, \quad (6)$$

which completely determine the dipole field for given length L_x . At fixed H_0 the limits $\eta \rightarrow 1$ and $\eta \gg 1$ correspond to nearly homogeneous and strongly inhomogeneous dipole magnetic fields in a cubic region of the simulation, respectively. Throughout this paper the cyclotron frequency Ω_b and the Alfvén velocity v_A are determined in terms of the magnetic field H_0 . It should be emphasized that the scheme outlined in Fig. 1 essentially differs from one adopted in [2, 20] where the dipole is located inside the simulation domain and due to the strong interactions the ions may be trapped by the dipole. The present model also essentially differs from our previous axially symmetric model [10] with $\mathbf{p} = p_x \mathbf{e}_x$ which allows 2D simulations.

The explosion forms a cloud of dense plasma of radius r_0 containing N_c ions with a total kinetic energy W_0 . At the initial time, the velocity of the cloud ions is distributed linearly along the radius, i.e. at $r < r_0$

$$v_r(r, 0) = u(r) = v_m \frac{r}{r_0} \quad (7)$$

and $v_r(r, 0) = 0$ at $r > r_0$. Here v_m is the maximal velocity of the ions in the cloud and is determined by the initial energy W_0 of the cloud, with $v_m = (10W_0/3N_c m_p)^{1/2} = v_0 (5/3)^{1/2}$, where

$v_0 = (2W_0/N_c m_p)^{1/2}$ is the average velocity of the cloud ions.

The equation of the energy conservation of the system is given by

$$W = W_{\text{kin}} + \int_{\Omega_{\text{sim}}} d\mathbf{r} \left(\frac{1}{2} n m v_e^2 + \frac{H^2}{8\pi} \right). \quad (8)$$

Here $n = n_e$, and n is the total density of the ions in the cloud and background plasmas. Ω_{sim} is the volume of the simulation box. The total energy of the system consists of the kinetic energies of the electron gas, the energy of the magnetic field, and the kinetic energy W_{kin} of the ions. Note that in Eq. (8) we have neglected the energy of the electric field as $v_e \ll c$ and $E \ll H$.

The system size employed in the computations is $L_x = L_y = L_z = 8.3a_L$ and uses $84 \times 84 \times 84$ cells in x, y, z directions, where $a_L = v_m / \Omega_b$ is the ion cyclotron radius. Thus, the cell size in the x, y, z directions is $h = 0.1a_L$. In order to correctly resolve the ion gyromotion the quantity h and the time step Δt are fraction of the ion cyclotron radius a_L and the ion cyclotron period Ω_b^{-1} , respectively. In our simulations $\Delta t = 0.01\Omega_b^{-1}$. The initial radius r_0 of the plasma cloud is considerably smaller than the step size h ; that is, we can assume that at the initial time the cloud is concentrated at a point. At the initial time $t = 0$ we take the background plasma at rest and assume that the background particles are distributed uniformly over the entire cubic region and the particles of the expanding plasma are distributed uniformly in the cloud. Explicitly the initial distribution functions of the background and cloud ions are given by $f_b(\mathbf{r}, \mathbf{v}, 0) = n_{b0} \delta(\mathbf{v})$ and $f_c(\mathbf{r}, \mathbf{v}, 0) = n_{c0} \delta(\mathbf{v} - u(r)(\mathbf{r}/r))$, respectively, where n_{c0} is the initial density of the cloud ions and $u(r)$ is determined by Eq. (7). Note that the distribution function $f_c(\mathbf{r}, \mathbf{v}, 0)$ is non-zero only at $0 \leq r \leq r_0$. Boundary conditions are one of the most important conditions to be satisfied in an electromagnetic problem, and they vary depending on the problem. In [2], periodic boundary conditions are imposed on the fields and the particles. They only run the system a relatively short amount of time before any disturbances reach the edges of the system. In this paper, at the boundaries of the cubic region $x = y = z = 0$ and $x = L_x, y = L_y, z = L_z$ all quantities are specified by its unperturbed values, and on the cloud-dipole axis (i.e. at $y = y_0, z = z_0$ and arbitrary x) we assume the condition $E_{yz} = H_{yz} = v_{ey,z} = 0$ which is a natural consequence of the symmetry of the model. The absorption boundary conditions are chosen for all the particles which mean that any particle leaving the computation domain is assumed to have gotten lost. With these boundary conditions the calculations are continued until the time the perturbations reach the boundaries of the cubic region.

The equations of motion for the ions are the equations of the characteristics of the Vlasov kinetic equation (1). Assuming hydrogen plasma we obtain

$$\dot{\mathbf{r}}_i = \mathbf{v}_i, \quad \dot{\mathbf{v}}_i = \frac{e}{m_p} \left(\mathbf{E} + \frac{1}{c} [\mathbf{v}_i \times \mathbf{H}] \right). \quad (9)$$

These equations are solved by the particle-in-cell (PIC) method using Boris pusher algorithm [36,37]. Instead of the kinetic equation integration, the trajectories of a large number of the quasi-particles (each of these particles in turn consist of the large number of ions) are computed. In our simulations the total number of the quasi-particles is 18.5×10^6 and 4.2×10^6 quasi-particles are used for a cloud. For the background plasma we set 16 quasi-particles in the cell with close values of the cyclotron radii (because $h \ll a_L$) which allows us to simulate ion kinetics in details. Further increasing the number of the quasi-particles does not essentially influence the simulation results. The Maxwell equations are solved using an explicit first order splitting scheme on staggered grid. A more detailed description of the mathematical model and the numerical simulation can be found, for example, in [35-37].

4. Results

In this section, results from several calculations are presented to describe the overall physics and to show the properties of the resulting structures. Numerical simulations have been performed for calculation of the energy, density and electromagnetic characteristics of the expansion of a hydrogen plasma into a uniform magnetized background hydrogen plasma at high Alfvén–Mach numbers with $M_A = v_m/v_a = 15.0$ and for a MLM interaction parameter $\delta = 0.71$. The basic physical parameters of the simulations are shown in Table, where $\tau_s = R_g/v_m$ is the hydrodynamic retardation time. Note that $R_g \ll R_m$ and the retardation of the cloud is caused here by the interaction with the background plasma. The dipole is placed at $x_d = -77.8$ cm (see Fig. 1). The initial radius of the plasma cloud is $r_0 = 0.01a_L$ which corresponds to the initial density $n_{c0} = 10^{20}$ cm⁻³. The parameter κ introduced in Sec. 2 is $\kappa > \kappa_c$. Thus we expect that the ions will not be captured by a dipole magnetic field. Using the parameters introduced above, the simulation is run to $t \approx 4.9\tau_s$ when the perturbation reach to the boundaries of the cubic region and the boundary conditions adopted here become invalid. The solutions of Eqs. (1)–(5) are obtained using the coordinate system shown in Fig. 1.

Figure 2 shows the time variation of the kinetic energies of the cloud and the background plasma. The energies are normalized to the initial energy of the plasma cloud W_0 and the time is given in units of the retardation time τ_s . It is seen that the energy of the plasma cloud decreases with

a time and at $t \approx 3.6\tau_s$, about a half of the initial energy is transferred to the background plasma. Let us recall that the Coulomb collisions between particles are completely ignored here and thus as mentioned in Sec. 2 the energy transfer is caused by the MLM interaction. In [32] a simple analytical model was suggested for the energy transfer from the plasma cloud to the ambient plasma in the presence of a homogeneous magnetic field. Assuming the initial distribution functions $f_c(\mathbf{r}, \mathbf{v}, 0) = N_c \delta(\mathbf{r}) f_0(v)$ and $f_b(\mathbf{r}, \mathbf{v}, 0) = n_b \delta(\mathbf{v})$ of the ions in the plasma cloud and the background plasma, respectively, the energy transfer in this model reads (see [32] for details)

$$\frac{\Delta W(t)}{W_0} = \frac{\delta}{6} \left[\kappa^5(t) + 5 \int_{\kappa(t)}^{\infty} \chi^2(x, t) dx \right], \quad (10)$$

where

$$\chi(x, t) = x^2 - \left[x^3 - \varphi\left(\frac{R_g x}{t}\right) \right]^{2/3} \quad (11)$$

$$\varphi(u) = 4\pi \int_u^{\infty} f_0(v) v^2 dv \quad (12)$$

Here the velocity distribution function $f_0(v)$ is normalized according to $\varphi(0) = 1$ and the quantity $\kappa(t)$ is determined from the transcendental equation

$$\kappa^3(t) = \varphi\left(\frac{R_g \kappa(t)}{t}\right). \quad (12)$$

Assuming that the strength of the homogeneous magnetic field is H_0 and the velocity distribution function $f_0(v) = (3/4\pi v_m^3) H(v_m - v)$ (where $H(z)$ is the Heaviside unit-step function) the prediction of this model is shown in Fig. 2a (the solid line). The transferred energy (10) at $t < \tau_s$ and for a chosen $f_0(v)$ is then given by $\Delta W(t)/W_0 \approx (\delta/6)(t/\tau_s)^5$ and in the limit $t \rightarrow \infty$ approaches $\Delta W_{\infty}/W_0 = C\delta$ (where $C \approx 0.59$) independently of the particles initial velocity distribution function in a cloud. It is seen that the theory agrees qualitatively with the simulation (squares) although it has been derived under assumption that $W(t) \ll W_0$. The sum of the cloud and background plasma energies is the total kinetic energy $W_{\text{kin}}(t)$ of the ions involved in the energy conservation relation, Eq. (8). This energy decreases with a time due to the energy transfer to the electrons (second term in Eq. (8)) and the magnetic field (last term in Eq. (8)). However, the amount of the energy gained by the electrons and the magnetic field is small compared to W_{kin} .

The time variation of the radial (W_r) and gyrorotational (W_{θ} , W_{ϕ}) components of the background plasma energy are shown in Fig. 2b. From the initial condition (7) it is clear that the radial and the gyrorotational energies of the plasma cloud at $t = 0$ are given by $W_r(0) = W_0$ and

$W_\theta(0) = W_\varphi(0) = 0$ and also there is neither radial nor gyromotion of the background particles. As shown in Fig. 2 the expanding plasma cloud loses its radial energy which is transferred to the gyromotion energy of the cloud and the background plasma ions. In addition a large amount of the cloud kinetic energy is transferred to the radial energy of the background ions.

The values of the parameters for the numerical simulation ($M_A = 15$, $S = 0.71$). The number of the ions (protons) in a cloud is $N_c = 1.67 \times 10^{19}$.

$a_L = 34.14$ cm	$R_g = 28.81$ cm	$R_m = 175.18$ cm	$\tau_s = 0.881$ μ s
$H_0 = 100$ G	$W_0 = 0.896$ kJ	$v_m = 3.27 \times 10^7$ cm/s	$\eta = 100$
$n_{b0} = 10^{14}$ cm $^{-3}$	$v_A = 2.18 \times 10^6$ cm/s	$\Omega_b = 9.58 \times 10^5$ s $^{-1}$	$\omega_{pb} = 1.32 \times 10^{10}$ s $^{-1}$

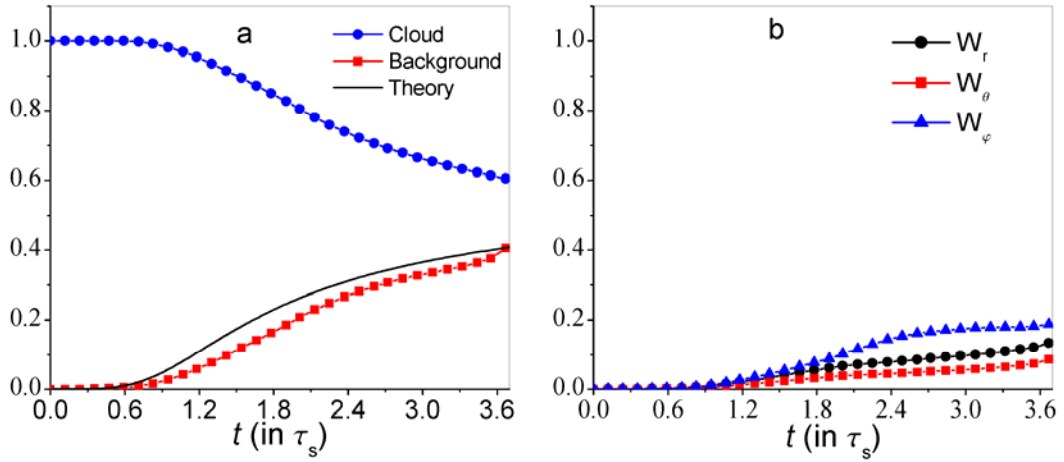


Fig. 2. The time (in units of τ_s) variation of the kinetic energy (in units of W_0) of the plasma cloud and background plasma particles for $M_A = 15.0$, $S = 0.71$. a) The variation of the total energy of the background plasma (squares) and plasma cloud (circles). The dashed line is the theoretical predictions of [32] (see the text for details). b) The time variation of the radial (W_r , circles) and the gyrorotational (W_θ , squares; W_φ , triangles) energies of the background plasma.

Figure 3 shows the distributions of the electric (first three columns) and the magnetic (last three columns) fields strengths in units of $(v_A/c)H_0$ and H_0 , respectively. Figure 4 shows the distributions of the densities of the cloud (first three columns) and the background plasma (last three columns) in units of n_{b0} at $t = \tau_s$, $t = 2.5\tau_s$, and $t = 3.5\tau_s$. As expected the density of the plasma cloud is strongly reduced due to the expansion. In addition the perturbations of the electromagnetic fields are larger at $\theta \sim 0$ where the dipole magnetic field is stronger. At the initial stage of the expansion process ($t \ll \tau_s$) the ions of the plasma cloud front propagates through a quiescent background plasma, and different plasmas are mixed. At this stage the background ions are accelerated mainly by the generated tangential (to the cloud surface) electric field. Then, turning under the Lorentz force action, they acquire the radial velocity. At the later stage when the radial and longitudinal electric fields arise, the motionless background ions acquire a velocity due to all components of the field. In general the motion of the ions in the electric and magnetic fields is very

complicated. They will do a gyromotion along the magnetic field lines. But along with the gyromotion, the ions will also experience $\mathbf{E} \times \mathbf{H}$ drift and gradient drift. The electric field is generated in a region of the perturbation of the magnetic field, and everywhere it is perpendicular to the total field \mathbf{H} .

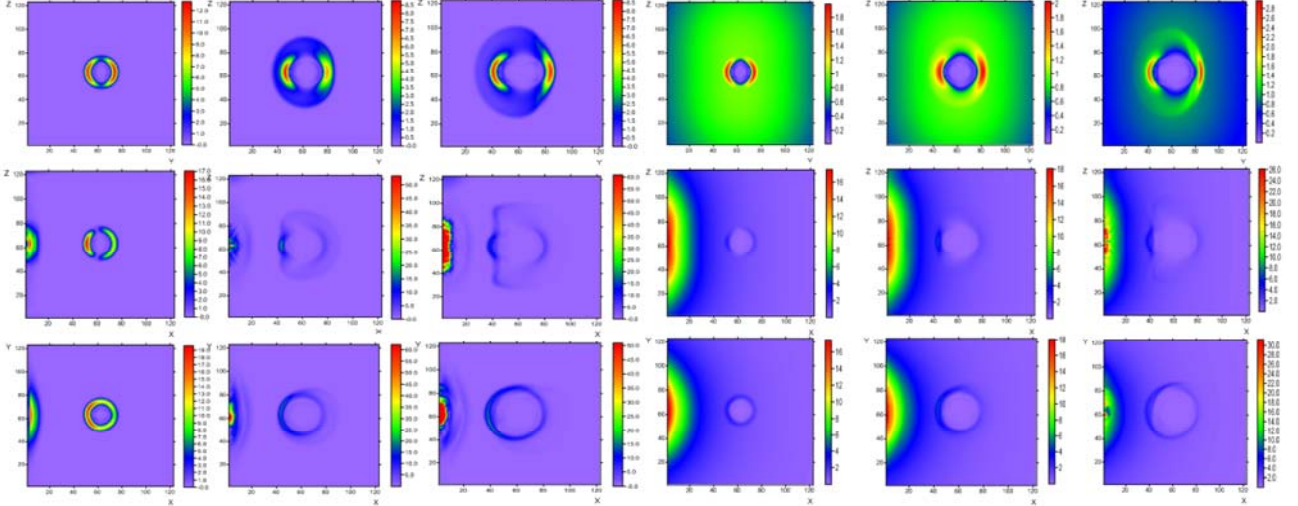


Fig. 3. The distribution of the electric (in units of $(v_A/c)H_0$, first three columns) and the magnetic fields (in units of H_0 , last three columns) at $t = \tau_s$ (first and fourth columns), $t = 2.5\tau_s$ (second and fifth columns) and $t = 3.5\tau_s$ (third and sixth columns). 2D figures were obtained for the planes which contain the center of the simulation box and are parallel to the planes $x = 0$ (first row), $y = 0$ (second row), and $z = 0$ (third row). The coordinates are given in units of $c/\omega_{pb} = 2.28$ cm.

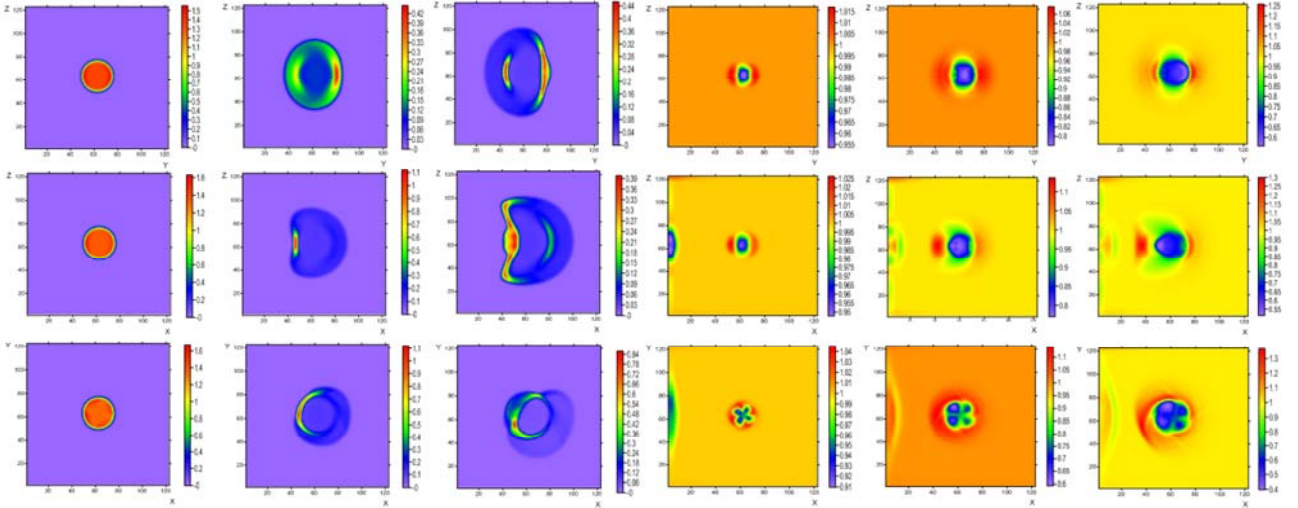


Fig. 4. 2D plots of the densities (in units of n_{b0}) of the plasma cloud (first three columns) and the background plasma (last three columns) at $t = \tau_s$ (first and fourth columns), $t = 2.5\tau_s$ (second and fifth columns), $t = 3.5\tau_s$ (third and sixth columns). Shown are the densities in the planes containing the plasma cloud center and parallel to the planes $x = 0$ (first row), $y = 0$ (second row), $z = 0$ (third row). The coordinates are scaled in $c/\omega_{pb} = 2.28$ cm (ω_{pb} is the plasma frequency of the background ions with the initial density $n_{b0} = 10^{14}$ cm $^{-3}$).

From Figs. 3 and 4 it is seen that the retardation of the plasma cloud is accompanied by the formation of a compressed plasma layer which moves together with the compressed electromagnetic field; i.e., a collisionless shock wave is formed. The depth of the compressed layer is of the order of the ion cyclotron radius a_L , in agreement with an estimate $\Delta \sim a_L$ of the width Δ

of the collisionless shock front given in [38]. The ions of the background plasma are pushed out of the expansion region; this leads to the formation of a plasma cavity. It correlates with the diamagnetic cavity, a region in which the total magnetic field $\mathbf{H}(\mathbf{r},t)$ is smaller than the unperturbed dipole field because it is squeezed out. Thus, there is essentially no electric field in the cavity. Due to the retardation of the ions of the plasma cloud front, a part of its mass forms a shell near the front boundary. However, this shell is not isotropic and is more visible at $\theta \sim 0$, i.e. in the region closer to the dipole. At the later time of the expansion $t \gtrsim \tau_s$, the plasma shell becomes more and more pronounced with the formation of the cavity also in the plasma cloud with sharply (with the width $\sim a_L$) distributed ions.

The time evolution of the plasma cloud boundary is shown in Fig. 4. As shown in this figure an initially symmetrical plasma cloud begins to be asymmetric in the $x = 0$ and $z = 0$ planes at $t \gtrsim \tau_s$. The similar shape of the plasma cloud is observed in the experiments as well as in numerical simulations of the plasma expansion in a vacuum when the background plasma is absent [1, 24]. In this case the asymmetrical pattern may be caused only by the ambient magnetic field. At the initial stage, the plasma cloud expands isotropically as a free stream with high kinetic energy. Then, plasma expanding in negative x -direction begins to decelerate because the ambient dipole magnetic field is stronger at a plane $x = 0$ near the dipole (see, e.g., Fig. 1). The kinetic beta β_c defined as the ratio of plasma cloud kinetic energy density to magnetic energy density reaches unity around this area first, and then strong interaction between plasma and the ambient field occurs. Thus, the diamagnetic motion of plasma is induced to generate the surface diamagnetic current asymmetrically, only on the plasma surface close to the dipole ($x = 0$ plane). In [39] (see also [40]) an analytical model was suggested to calculate the pressure of the dipole magnetic field on the surface of the plasma cloud. It was shown that at $\mathbf{p} = p_z \mathbf{e}_z$ this pressure vanishes at $\varphi \approx 0; \pi$ and has its maximum at $\varphi \approx \pi/2$ and $\varphi \approx 3\pi/2$. Therefore this layer of the expanding plasma sphere will be mainly deformed by the external magnetic pressure. In the present context of the high-energy expansion $\beta_c \gg 1$ even at the later stages of the expansion and the magnetic field cannot deform directly the cloud shape. In this case the deformation occurs due to the interaction with the background plasma with initially low kinetic β_b . Then the background plasma tends to change the shape to follow the dipole magnetic field lines. As shown in Fig. 2 the kinetic energy of the background ions and hence the parameter β_b increases with time which leads to the formation of the asymmetrical kinetic pressure of the background ions on the plasma cloud.

The asymmetry of the plasma cloud in the plane containing its center and parallel to the yz plane (Fig. 4, first row) is particularly noteworthy. It should be emphasized that the dipole magnetic field is symmetric in this plane with respect to the vector $\mathbf{p} = p_z \mathbf{e}_z$ and the asymmetry cannot be

observed in the simulations with a genuinely 2D geometry [10]. Our calculations show that such an asymmetry is caused by the gyrorotational behavior (note that $\Omega_b \tau_s \approx 1$) of the plasma and as a consequence by the generation of the vortical structures in a low-energy background plasma (Fig. 4, third row). The mechanism of the interaction of these vortices with the plasma cloud is the same as discussed above. This is an interesting issue which we intend to address in a more detailed forthcoming studies.

5. Conclusions

In this paper we have investigated the collisionless expansion of the dense plasma cloud into magnetized background plasma in the presence of a dipole magnetic field. The 3D hybrid-PIC simulations with kinetic ions and massless fluid electrons have been employed. We have considered the case of high-energy super-Alfvénic expansion with $M_A \gg 1$ when the expanding plasma is not captured by the ambient magnetic field. It is shown that in this parameter regime the retardation and the deformation of the plasma cloud is mainly caused by the interaction with background plasma which, however, can be strongly affected (at least at the initial stage) by a magnetic field. Our numerical results for the energy transfer from the plasma cloud to the background plasma have been compared with the theoretical predictions of [32] and qualitatively good agreement has been found. For future applications the arbitrary orientation of the dipole (with respect to the x , y , and z -axes, see Fig. 1) should be considered. For instance, such a configuration has been realized in the experiment [24]. In this case the the shape of the plasma cloud may become strongly asymmetric in all directions.

An additional item for further investigations is the development of a model which accounts the thermal effects for electrons which are completely neglected in the current study. These effects can be included by adding in the right hand side of Eq. (5) the term $-(1/en)\nabla p_e$, where p_e is the thermal pressure of the electrons. Also along with Eqs. (1)–(5) an equation for the evolution of p_e should be considered (see, e.g., [9]). In this connection assuming the strong heating of the electrons in the shock front it is also desirable to investigate the physics allowing for charge separation effects and the resolution of the electron Debye length scale. We intend to address this and other issues in the context of the plasma expansion in a separate study.

Acknowledgments

This work was made possible in part by a research grant (Project PS-2183) from the Armenian National Science and Education Fund (ANSEF) based in New York, USA. Also this work has been partially supported by the Armenian Ministry of Higher Education and Science (Project No. 11-1c317).

REFERENCES

1. **Yu.P.Zakharov**, IEEE Trans. Plasma Sci., **31**, 1243 (2003).
2. **D.Winske, N.Omidi**, Phys. Plasmas, **12**, 072514 (2005).
3. **R.M.Winglee, J.Slough, T.Ziemba, A.Goodson**, J. Geophys. Res.: Space Phys., **105**, 21067 (2000).
4. **R.M.Winglee**, Geophys. Res. Lett. **25**, 4441 (1998).
5. **B.H.Ripin, J.D.Huba, E.A.McLean, C.K.Manka, T.Peyser, H.R.Burris, J.Grun**, Phys. Fluids B, **5**, 3491 (1993).
6. **R.P.Drake**, Phys. Plasmas, **9**, 727 (2002).
7. **D.Winske**, J. Geophys Res.: Space Phys., **93**, 2539 (1988).
8. **S.H.Brecht, V.A.Thomas**, J. Geophys. Res.: Space Phys., **92**, 2289 (1987).
9. **D.A.Osipyan, H.B.Nersisyan, H.H.Matevosyan**, Astrophysics, **46**, 434 (2003).
10. **H.B.Nersisyan, D.A.Osipyan**, Contrib. Plasma Phys., **49**, 351 (2009).
11. **J.D.Huba, P.A.Bernhardt, J.G.Lyon**, J. Geophys. Res., Space Phys., **97**, 11 (1992).
12. **G.Gisler**, IEEE Trans. Plasma Sci., **17**, 210 (1989).
13. **D.Winske**, Phys. Fluids B, **1**, 1900 (1989).
14. **J.D.Huba, A.B.Hassan, D.Winske**, Phys. Fluids B, **2**, 1676 (1990).
15. **S.H.Brecht, N.T.Gladd**, IEEE Trans. Plasma Sci., **20**, 678 (1992).
16. **J.H.Oort**, Mon. Notic. Roy. Astron. Soc., **106**, 159 (1946).
17. **I.S.Shklovskii**, Supernova Stars and Processes Associated with Them, Moscow: Nauka, 1976 (in Russian).
18. **R.M.Winglee, P.Euripides, T.Ziemba, J.Slough, L.Giersch**, AIAA/ASME/SAE/ASEE Joint Propulsion Conference and Exhibition, Huntsville, AL, 2003 (AIAA, 2003), Paper 2003-5224.
19. **D.E.Parks, I.Katz**, J. Spacecr. Rockets, **40**, 597 (2003).
20. **H.B.Tang, J.Yao, H.X.Wang, Y.Liu**, Phys. Plasmas, **14**, 053502 (2007).
21. **L.Gargate, R.Bingham, R.A.Fonseca, R.Bamford, A.Thornton, K.Gibson, J.Bradford, L.O.Silva**, Plasma Phys. Control. Fusion, **50**, 074017 (2008).
22. **R.M.Winglee, T.Ziemba, J.Slough, P.Euripides, D.Gallagher**, Space Technology and Applications International Forum (STAIF- 2000) on Space Exploration and Transportation-Journey into the Future, Albuquerque, NM, 2001 AIP Conf. Proc., no. 552, AIP, New York, 2001, p. 407.
23. **R.M.Winglee, T.Ziemba, P.Euripides, J.Slough**, Space Technology and Applications International Forum, STAIF-2002, Conference on Innovation Transportation Systems for Exploration of the Solar System and Beyond, Albuquerque, NM, 2002 AIP Conf. Proc. no. 608, AIP, NY, 2002, p. 443.
24. **T.Muranaka, H.Uchimura, H.Nakashima, Yu.P.Zakharov, S.A.Nikitin, A.G.Ponomarenko**, Jpn. J. Appl. Phys., **40**, 824 (2001); **K.V.Vchivkov, H.Nakashima, Yu.P.Zakharov, T.Esaki, T.Kawano, T.Muranaka**, Jpn. J. Appl. Phys., **42**, 6590 (2003).
25. **Yu.P.Raizer**, Soviet J. Appl. Mech. Tech. Phys., **6**, 19 (1963).
26. **Yu.P.Zakharov, A.M.Orishich, A.G.Ponomarenko**, Laser-Produced Plasma and Laboratory Simulation of Non-Stationary Space Processes (in Russian), Ed. **N.G.Preobrazhensky**, Inst. Pure and Applied Mechanics, Novosibirsk, 1988.
27. **B.A.Trubnikov**, Particles Collisions in Completely Ionized Plasma, in: Reviews of Plasma Physics, Ed. **M.A.Leontovich**, New York: Consultants Bureau, **1**, 105 (1965).
28. **D.W.Koopman**, Phys. Fluids, **15**, 1959 (1972).
29. **Yu.P.Raizer, S.T.Surzhikov**, AIAA Journal, **33**, 486 (1995); **Yu.P.Raizer, S.T.Surzhikov**, AIAA Journal, **33**, 479 (1995).

30. **C.S.Wu, D.Winske, Y.M.Zhou, S.T.Tsai, P.Rodriguez, M.Tanaka, K.Papadopoulos, K.Akimoto, C.S.Lin, M.M.Leroy, C.C.Goodrich**, Space Sci. Rev., **37**, 63 (1984).
31. **K.Papadopoulos**, J. Geophys. Res., **14**, 3806 (1971).
32. **A.I.Golubev, A.A.Solov'ev, V.A.Terekhin**, J. Appl. Mech. Tech. Phys., **19**, 602 (1978); **V.P.Bashurin, A.I.Golubev, V.A.Terekhin**, J. Appl. Mech. Tech. Phys., **24**, 614 (1983).
33. **S.A.Nikitin, A.G.Ponomarenko**, J. Appl. Mech. Tech. Phys., **34**, 745 (1993).
34. **G.Haerendel, R.Z.Sagdeev**, Artificial Plasma Jet in the Ionosphere, in: Advances in Space Research, **1**, 29 (1981).
35. **M.M.Leroy**, Computer Simulations of Collisionless Shock Waves, in: Advances in Space Research, **4**, 231 (1984).
36. **R.W.Hockney, J.W.Eastwood**, Computer Simulation Using Particles, CRC Press, 1988.
37. **C.K.Birdsall, A.B.Langdon**, Plasma Physics via Computer Simulation, Taylor and Francis, 2004.
38. **R.Z.Sagdeev**, Cooperative Processes and Shock Waves in Rarefied Plasmas, in: Reviews of Plasma Physics, Ed. **M.A.Leontovich**, New York: Consultants Bureau, **4**, 23 (1966).
39. **H.B.Nersisyan, D.A.Osipyan**, J. Phys. A: Math. General, **39**, 7531 (2006).
40. **H.B.Nersisyan**, Phys. Lett. A, **374**, 4049 (2010).